RSC Advances

ROYAL SOCIETY OF CHEMISTRY

www.rsc.org/advances

Role of Substrate Purity and its Crystallographic Orientation on the Defect Density of Chemical Vapor Deposition Grown Monolayer Graphene

Munu Borah[a,b], Dilip K. Singh[a], Kiran M. Subhedar [a] and Sanjay R. Dhakate[a,b]*

[a] Physics and Engineering of Carbon, Division of Material Physics and Engineering,
CSIR-National Physical Laboratory, New Delhi-110012, India

[b] *Academy of Scientific & Innovative Research(AcSIR), CSIR-NPL Campus, New Delhi-110012*

Abstract

Defect free mono-layer graphene sheet growth has remained a challenge towards its huge potential applications in electronic and photonic devices. Here, we are reporting about role of copper substrate's purity and its crystallographic orientation on the quality of graphene grown using low pressure chemical vapor deposition technique. Graphene is grown on three different purities (Cu-I, Cu-II and Cu-III) substrates under analogous conditions of optimized pre-growth annealing and cleaning process. Irrespective of purity level of all the substrates, it demonstrates that monolayer graphene ($I_{G'}/I_G \sim 4$) with different defect density is observed. The amount of defects and defect density in the three samples is correlated with the different lattice planes of Cu, which are participating during growth process. The size of lattice grain advance upon annealing is observed and it is substrate purity dependent. It reveals that graphene growth is favored by either (111) or (100) plane or both. It demonstrated that role of substrate's purity is extremely accountable for growth of defect free monolayer graphene for device applications which required ballistic transport properties.

* Corresponding author: dhakate@mail.nplindia.org (Telephone no. +91-11-4560-9388)

Introduction

Synthesis of large area defect free graphene for device fabrication suggest that key to control the growth parameter still remains unknown and uncontrolled[1-4]. In spite of number of attempts to reveal the parameters of defect free graphene growth, consensus about defect free graphene growth has not been so far reached graphene having theoretically predicted transport properties. Graphene is predicted to show relativistic transport properties with electron mobility as high as 200,000 $cm^2\ V^{-1}\ s^{-1}$ [5]with ability to sustain very high current density (million times higher than that of Copper) [6] and electrical conductivity 2×10^3 S/cm[7] with zero effective mass[8]. Whereas in contrast to theoretical predictions, experiment shows widely varying values of carrier mobility of ~ 4000 - 8000 $cm^2\ V^{-1}\ s^{-1}$ which is roughly three order of magnitude lesser than the theoretical prediction[6-8]. A number of techniques has been attempted to grow graphene like mechanical exfoliation of graphite[9], epitaxial growth on SiC[10], chemical reduction of exfoliated graphene oxide[11] and chemical vapor deposition (CVD)[12]. Li and colleagues for the first time demonstrated CVD based growth in 2009[13]. CVD based graphene growth is cost effective and can be used to grow large size sheets[12] while mechanical exfoliation is a time consuming process and mostly gives small size graphene sheet. SiC based growth is a commercially nonviable technique. Till date the best possible mobility in case of CVD based graphene in an average ~3000 $cm^2V^{-1}S^{-1}$[14] while other two techniques shows much higher values of electron mobility ~5000[15]and ~6450 $cm^2V^{-1}S^{-1}$[16]. Currently dendritic growth, formation of multilayer, and the lower carrier mobility are issues of concern among researchers working with CVD based graphene growth[17, 18]. Attempts has been made by growing graphene on various transition metal and their alloys[19, 20] on P-block elements (Ga), using liquid Cu surface[21, 22] and on Copper substrate with Chromium oxide coating[23].

A number of physical parameter like gas flow rates, nature of the substrate and thermodynamic parameters are expected to play crucial role towards quality of graphene grown[24]. In recent studies, the effect of substrate on growth rate and uniformity of graphene has been primarily addressed. In case of polycrystalline copper substrate, a more favorable growth has been observed from Cu (111) plane than that of Cu (100) for uniform monolayer graphene synthesis[25]. In contrast to it, Rasool et al[26] have reported that the quality of graphene is controlled by the active sites of nucleation rather than the atomic structure of the copper substrate, also (100)

established as more preferential. Whereas Wood et al.(2011) studied the growth through Electron Back Scattering Diffraction (EBSD) and observed that for perfect graphene sheet growth in Cu(111) plane than that of Cu(100)[27]. Although the growth of defect free graphene over Cu-substrates with different crystallographic orientation Cu (100) or Cu(111) plane is largely debated, but role of substrate's purity and evolution of various crystallographic orientations during pre-growth annealing process has not been experimentally explored in a broad sense. Vlassiouk et al [28] have studied on the morphology and size of graphene domains with varying partial pressure of CH_4 and H_2. They have performed their experiment by using two different Cu substrate namely low (99.8%, Alfa Aesar) and high (99.999%, Alfa Aesar) respectively. Similarly Liu et al [29] also have concluded from their work on monolayer graphene synthesis by CVD, that the partial pressure of hydrocarbon and purity of copper substrate plays important role on determining the uniformity of graphene layer by CVD. Controlled growth need to address issues like nucleation density, surface adsorption mechanism of carbon atom over substrate, crystallinity and purity of substrate used[30]. Additionally various factors during post growth transfer processes also affects the quality of graphene in terms of its sheet resistance and charge mobility like cracks and wrinkles originated along the grain boundaries during transfer process[31]. In this paper, we report about the role of substrate purity and its crystallographic orientation towards the quality of graphene grown.

Experimental Section

Graphene sheets were grown on three types of Cu, namely Cu-I, Cu-II and Cu-III with purity and thickness 99% (50 μm), 99.8% and 99.999% pure (25 μm) procured from Klim and Alfa Aesar respectively. The impurities present in the copper includes different concentration of Al, K, Si, C, Li, Ti, Fe, Na, I and S as specified by the supplier. The gases argon (Ar), hydrogen (H_2) and methane (CH_4) of 99.9% purity were used for growth. Acetone (99.5% purity), iso propyle alcohol (IPA 99.7% purity), acetic acid (99.8% purity), poly- methyl methacrylate (PMMA), chlorobenzene (99% purity) and ammonium persulfate (98% purity) were obtained from Sigma-Aldrich.

Copper Substrate Cleaning:

Cu foils were kept in acetone and ultrasonicated for 1 minute and air dried under flow of nitrogen. Further, it was sonicated in Iso-propyl Alcohol for 1 min and again air dried. After cleaning copper foils were soaked in acetic acid and mildly sonicated for 10 minutes at low frequency. High frequency sonication was purposely avoided to stop formation of non-uniform wrinkled surface. After sonication it was washed repeatedly with deionized water. Finally, the foils were again cleaned with IPA and allowed for air-drying under flow of nitrogen.

Graphene growth in CVD:

Graphene sheets were synthesized using single zone tubular split furnace with horizontal quartz reactor of length 1.25 m and internal diameter of 80 mm, schematically shown in Figure S1(supplementary information). Gas flow rate was controlled using electronic mass flow controllers AALBORG, USA.

All the three different Cu foils were placed on quartz substrate and kept in the central isothermal zone of the furnace which was heated up to 1000 ºC in H_2 and Ar gas atmosphere at flow rate 4 sccm and 15 sccm respectively (total pressure 0.135 torr) into the system. The foils were annealed for 30 min to remove residual oxide so as to smooth the surface for the growth and subsequently CH_4 gas was introduced as carbon precursor at flow rate 25 sccm for 10 min, in presence of H_2 (total pressure 0.29 torr). After growth, samples were cooled to room temperature at cooling rate 25 °C/min under Ar and H_2 atmosphere see supplementary information (Figure S1). The growth was attempted on number of substrates before arriving to the conclusions.

Transfer process of graphene:

The PMMA solution prepared by dissolving 4.6g of PMMA in 100 ml chlorobenzene was coated on the graphene films by spin coater (Spin NXG-P1, Apex Equipment). PMMA coated sample was kept on hot plate for 1 min at 180 ºC for baking. For etching of Cu from graphene, PMMA coated graphene film was kept in an aqueous solution of 20 gm of ammonium persulfate ($H_8N_2O_8S_2$) in deionized water. After complete etching of Cu within 8-10 hours, the resultant sample was transfer onto the final silicon substrate followed by soaking in an acetone solution for the removal of polymer coating from graphene sheet.

Characterization:

Optical microscopy (Zeiss Axiolab A1) was performed to study the evolution of grain boundaries on before / after annealed copper substrates as well as on graphene grown substrate. Raman spectra of graphene was taken by Reninshaw spectrophotometer (micro-Raman model inVia Reflex) with 514 nm laser excitation. For Raman spectra 50× (NA 0.75) objective was used with laser power of 5 mW (laser spot size ~ 0.8μm).

The crystal structure of copper foil before and after annealing and graphene-copper samples were studied by X-ray diffraction (XRD, D–8 Advanced Bruker diffractometer) using CuK_α radiation (λ = 1.5418 Å).

The surface morphology of as grown graphene on copper substrate was observed by scanning electron microscope by back scattering mode (SEM, VP-EVO, MA-10, Carl-Zeiss, UK) operating at an accelerating potential of 10.0 kV.

Results and Discussions:

Fig 1 (a)-(c) shows the typical optical micrographs of three different copper foils (Cu-I, Cu-II, Cu-III) of different purity after cleaning. The bare copper foil consist of different orientation of grains on the surface (appearing as parallel lines in optical micrograph), see Fig 1 (a-c). These

grains on the surface arise from the processing and also due to the difference in the purity of copper. The initial orientation of grains and internal stress within the foil are expected to influence the evolution of grain size and orientation during annealing.

The copper substrates was chemically cleaned and subsequently annealed at 1000 ºC under flow of mixture of Ar and H_2 gas (4:1) to remove native oxide layer and smoothen the surface. The substrates were annealed for 30 min, 45 min and 60 min to monitor the evolution of randomly curved grain boundaries as shown in Fig. 1(d-l). Fig. 1 (d) shows co-existence of large and small grains in Cu-I (i.e twin formation). This indicates the occurrences of secondary grain growth in Cu-I upon annealing. Fig. 1(d) and 1 (f) shows defined regions of grain boundaries formation for Cu-I and Cu-III annealed for different periods, while Cu-II shows formation of elongated open grain boundaries Fig. 1(e). A single large twin forms and grows upon annealing so that a portion of the original boundary is replaced by an immobile coherent twin boundary and a mobile incoherent boundary when surface energy considerations are favorable resulting in large size grain growth in case of Cu-I and Cu-III upon annealing. While in case of Cu-II upon annealing formation of open ended long grain boundaries results due to unfavorable surface energy considerations[32]. It is clear that substrate with higher purity i.e Cu-III shows larger size grain growth after annealing for 30 min, 45 min and 60 min as shown in Fig. 1(f), (i) and (l) respectively compared to Cu-I and Cu-II. With increasing annealing time from 30 minutes to 45 minutes, the size of the grain boundaries increases. While further increase in the annealing period to 60 minutes, leads to formation of ripples and regions of increased surface roughness which appears as dark patches was observed in optical microscope (see in Fig. 1 (j) and Fig. (l)). The 30 min annealing is found to be the most suitable condition of pre-growth annealing from X-ray diffraction studies shown in Fig. S1 (supplementary information). Although the grain size

increase with increasing annealing time from 30 mins to 60 mins, the preferred planes of growth (111) and (100) shows monotonically decreasing intensity in X-ray diffraction pattern along with surface degradation in terms of roughness. Optically the substrate with low purity Cu-I shows relatively lesser change in surface roughness as compare to Cu-II and Cu-III upon 60 mins of annealing. This is due to higher melting temperature for substrate with higher impurity (i.e Cu-metal alloys) and also due to high thickness of substrate Cu-I as compared to Cu-II and Cu-III.

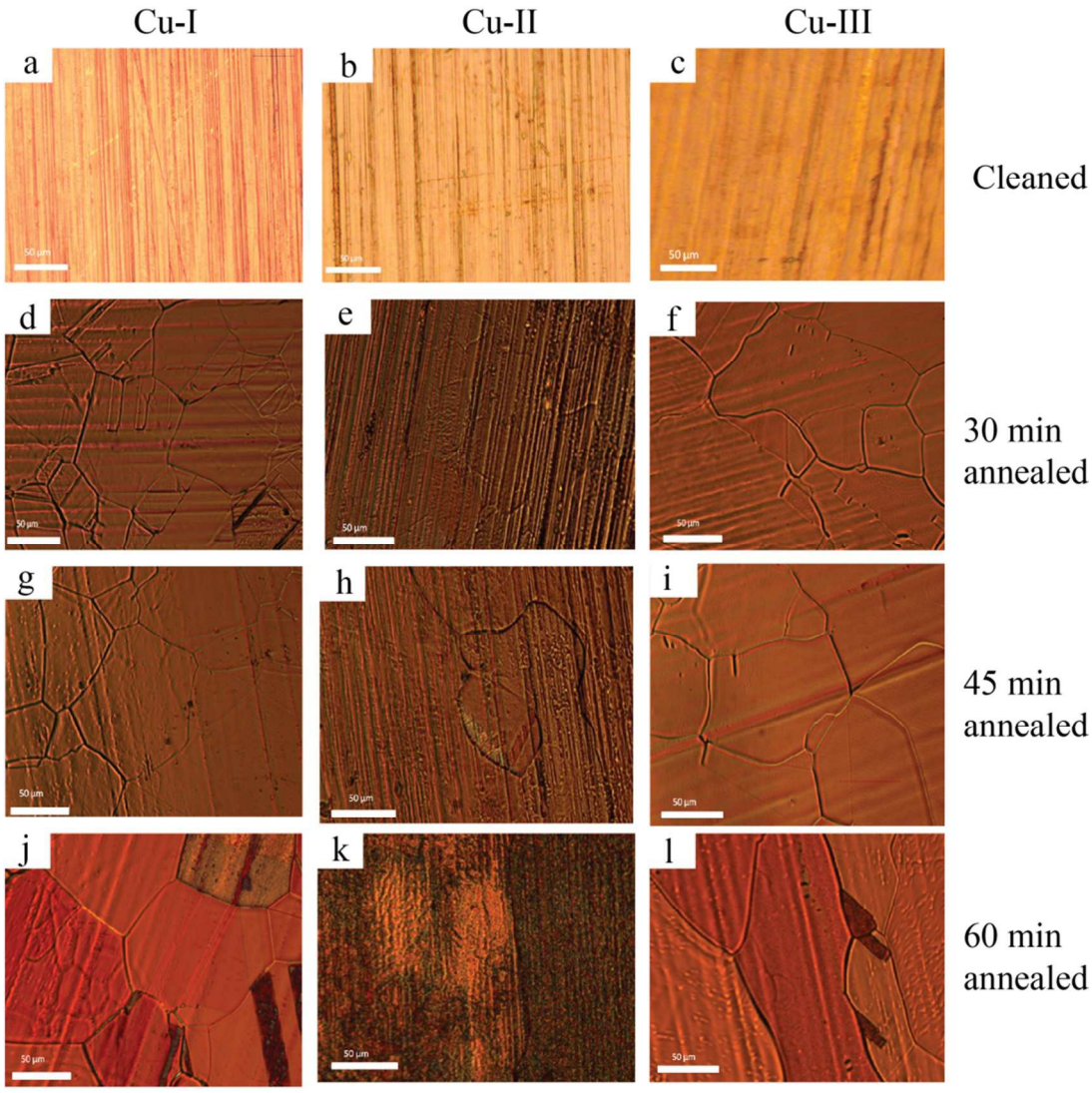

Fig 1: Optical micrographs of copper substrate after annealing at 1000°C for 30 min, 45min, and 60 min respectively. Cu-I (a-c), Cu-II (d-f) and Cu-III (g-i).

Fig. 2 shows the optical images (Fig. 2a-c) and SEM micrographs (Fig. 2 d-f) of graphene grown for 10 mins on Cu substrate. The substrates were annealed at 1000ºC for 30 min before growth. During growth, the curvature of grain boundaries on Cu substrate increases adsorption energy of incoming carbon atoms and acts as nucleation sites helping in formation of longer strip like graphene[33]. In Fig. 2 (a) and Fig. 2(c), optical images demonstrate the restricted growth within closed regions of grain boundaries apparent from restricted regions of similar contrast.

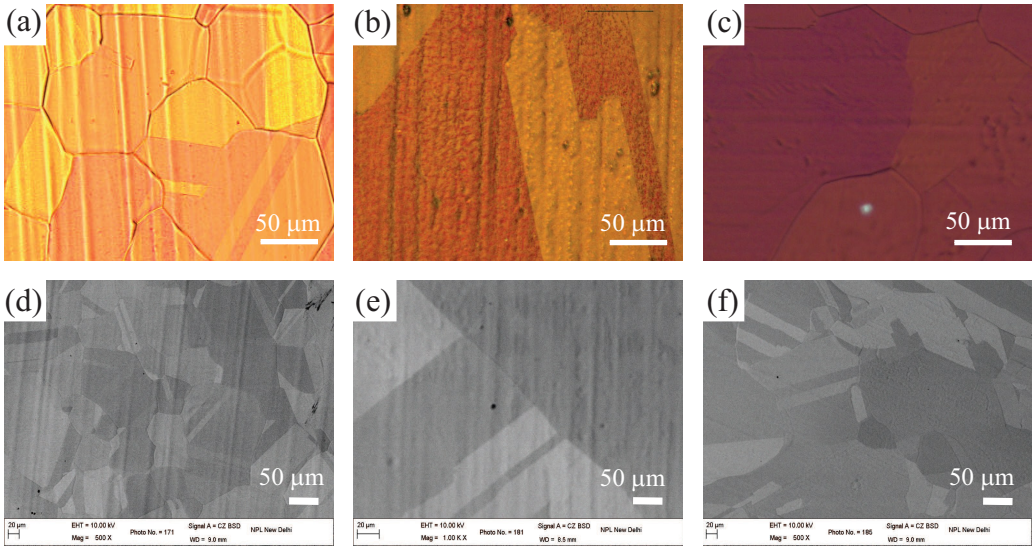

Fig 2: Optical microscopy image of graphene grown on copper substrate (a) Cu-I, (b) cu-II and (c) cu-III. SEM-back scattering image of graphene on (d) Cu-I, (e) cu-II and (f) cu-III grown by LPCVD at 1000°C

Fig. 2 (d), (e) and (f) shows SEM backscattering images of graphene grown for 10 mins on annealed copper substrates. Since metallic substrate Cu is expected to shows relatively stronger elastic backscattering of electrons and hence it appears as light contrast compared to the grown graphene. Fig.3 (a)-(c) shows the optical micrographs of transferred graphene on SiO_2/Si substrate grown on Cu-substrate of three different purity Cu-I, Cu-II and Cu-III respectively. The approximate area of the continuous graphene film synthesized by using three different substrate are Cu-I ~ 0.926, Cu-II ~ 0.718 and Cu-III ~ 0.569 mm^2 in Fig 3(a)-3(c). Graphene transferred from Cu-I show relatively larger regions of folded and agglomerated morphology as compared to transfer from Cu-II and Cu-III, see Fig. 3(a)-(c). Fig. 3 (d) shows Raman spectra of transferred

graphene sheets from three substrates of different purity. Raman spectra show three prominent features at ~ 1347, 1584 and at ~ 2685 cm^{-1} known as D-band, G-band and G´ band respectively.

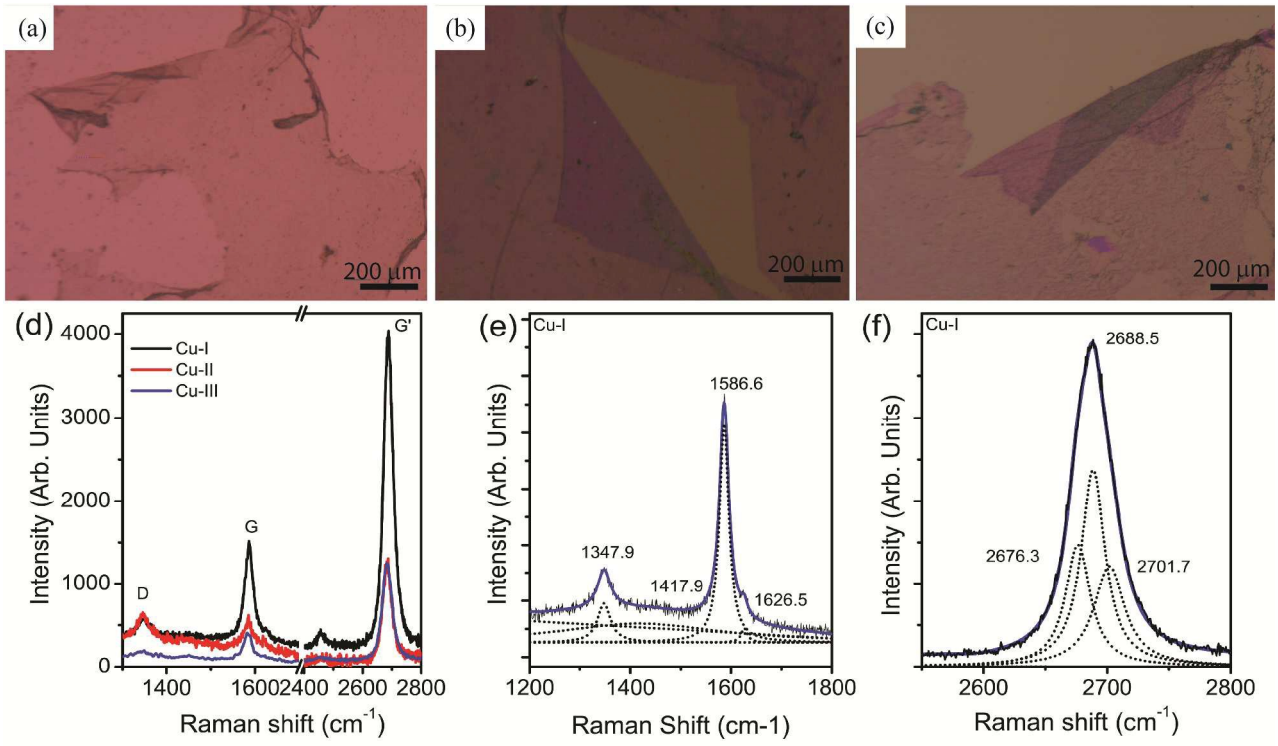

Fig. 3: Optical image of transfer graphene sheet on SiO_2/Si substrate, which is grown on (a) Cu-I, (b) Cu-II and (c) Cu-III. (d) Raman spectra of transferred graphene onto SiO_2/Si substrate that is synthesized on three Cu substrate of different purity. (e) Lorentzian fit to D and G peaks of Cu-I grpahene and (f) Lorentzian fit for G´ peak of Cu-I graphene.

These spectra are fitted with Lorentzian line shape and corresponding spectra information's related to all the three types graphene is enlisted in Table –1. A typical fitting for sample transferred from Cu-I substrate (referred as Cu-I graphene) is shown in Fig. 3(e) for D and G peak and in Fig. 3 (f) for G´ band separately for clarity. Cu-I and Cu-II shows D-band at ~ 1347 cm^{-1} with FWHM ~ 31 cm^{-1}. While Cu-III graphene shows D-band at 1345 cm^{-1} with almost double peak-width. Cu-II graphene shows the highest peak intensity of the D-band 295 counts while the Cu-I graphene shows 206 counts and Cu-III graphene shows the lowest intensity 81 counts. The difference in the peak width of Cu-III possibly arises due to the presence of more disordered carbon in Cu-III surface with lowest density, while Cu-I and Cu-II contains localized defects. The G-band position shifts monotonically from 1586.6 to 1584.9 and 1582.9 cm^{-1} i.e.,

towards lower Raman shift with increasing Cu purity. This indicates higher strain in grown graphene with increasing purity of Cu substrate.

Table-1: Raman spectra line profile parameters of graphene grown on Cu substrate of different purity Cu-I, Cu-II and Cu-III.

Sample	D peak position (cm^{-1})	G peak position (cm^{-1})	G´ peak Position (cm^{-1})	G´-FWHM (cm^{-1})	$I_{G'}/I_G$	I_D/I_G
Cu-I	1347	1586	2688	23.5	3.7	0.2
Cu-II	1347	1584	2685	21.2	3.9	0.9
Cu-III	1345	1582	2683	24.4	3.5	0.3

The G band shows nearly same peak width in case of graphene grown on Cu-I and Cu-III substrates nearly 22 cm^{-1}, while Cu-II graphene shows peak width of about 28 cm^{-1}. Higher peak width observed in case of Cu-II graphene is in agreement with higher D-band intensity observed for it, indicating presence of highest defect density compared to other two samples Cu-I and Cu-III. The second order G´ mode shows nearly fourfold intensity than the first-order graphitic G peak for all the three samples as expected from the single layered graphene structure[34]. In case of graphene, intense second-order G´ mode arises due to the inter-valley double resonance Raman scattering[35-37]. Fitting with Lorentzian line shape shows three components of G´ peak as observed earlier by Dresselhaus et al. The three peak structure arises due to two phonon assisted second order Raman scattering process[38]. In the two photon inter-valley scattering process two high symmetry points K and K´ of the first brillouin zone of the graphene participates. Out of four possible phonon assisted transition between valence band and conduction band two are degenerate resulting into three peak structure of G´ band[38]. The G´ band shows blue-shift with increasing purity of Cu substrate. Graphene grown on Cu-I foil (low purity 99%) shows G´ peak at 2688 cm^{-1}, grown on Cu-II at 2685 cm^{-1} and grown on Cu-III at 2683 cm^{-1}. The observed shift in the G´ peak position with purity of copper substrate is in agreement with shifts registered for G band. The quality of the graphene grown is usually expressed in terms of $I_{G'}/I_G$ intensity ratio while I_D/I_G (the defect ratio) and FWHM of G´ gives information about the number of layer and defect intensity present in graphene[34, 39]. The electronic band structure around the Fermi level for

multilayer graphene plays an important role in an inter valley double resonance Raman[35]. The three samples Cu-I graphene, Cu-II graphene and C-III graphene shows almost similar $I_{G'}/I_G$ ratio 3.7, 3.9 and 3.5 with varying I_D/I_G ratio 0.2, 0.9 and 0.3 respectively. The ratio of $I_{G'}/I_G$ is highest in case of graphene grown on Cu-II substrate as compared to Cu-I and Cu-III. The ratio I_D/I_G of defect density in the synthesized graphene is highest in case of graphene grown on Cu-II. This indicates Cu-II favors highly crystalline graphene with relatively more localized defects. We have also measured the defect density (n_D) from the Raman intensity profile using empirical relations presented by Cancado et al. [40].

$$n_D\,(\mu m^{-2}) = (1.8\pm0.5)/\,\lambda_L^{\,4} \times 10^{14}\,(I_D/I_G)$$

Average defect density of graphene grown on Cu-I, Cu-II and Cu-III substrate are found to be 515.76, 2320.93 and 773.64 μm^{-2} respectively. Defect density (n_D) is inversely proportional to the square of inter defect distance [41] and the corresponding I_D/I_G for a specific inter defect distance (L_D), depends on the laser energy [40 42]. Defect density estimates the limit of graphene mobility. The defect density present is correlated with the crystal plane of the substrate used for graphene growth. For instance graphene grown on Cu-II substrate hold the highest defect density in comparison to other substrates, Cu-I and Cu-III. It may be due to the presence of specific crystallographic plane participating on the graphene growth as discussed in XRD analysis in subsequent section.

Further, observations are validated by Raman spectroscopy analysis at various locations over the samples as shown in Fig. 4. Fig. 4(a) to (c) show the optical micrographs and marked points at which the spectra was recorded for Cu-I graphene, Cu-II graphene and Cu-III graphene sheet. The corresponding spectra are depicted in Fig. 4(d), 4(e) and 4(f) for Cu-I graphene, Cu-II graphene and Cu-III graphene, numbered sequentially as the spot positions. It reveals monolayer graphene growth with discontinuity as reflected by various regions with ratio $I_{G'}/I_G > 3$ and equally many other points showing absence of characteristic features. Fig. 4 (e) and 4(f) shows Raman spectra taken over various points for Cu-II and Cu-III graphene. The Raman spectra measured over unfolded region confirms growth of single layer graphene ($I_{G'}/I_G \approx 3$)[43 44] Whereas, in folded regions $I_{G'}/I_G$ ratio is < 2. Additionally, in the folded regions the G´ and G

peak appears at different Raman shifts, due to their similarity in behavior with bi-layer or few layer graphene [45]. Similarly, I_D/I_G ratio is different in case of folded and unfolded regions. It is nearly double in case of folded region as compared to unfolded region. One of the possible sources of high D-band intensity in case of folded regions is deformation of 2D graphene structure due to left out residual PMMA during transfer process. The Raman spectroscopic measurement at various points of Cu-III graphene shows that it has high crystallinity monolayer structure (max $I_{G'}/I_G$ =4.24) with a very low defect density even in folded regions (Fig. 4 (f)).

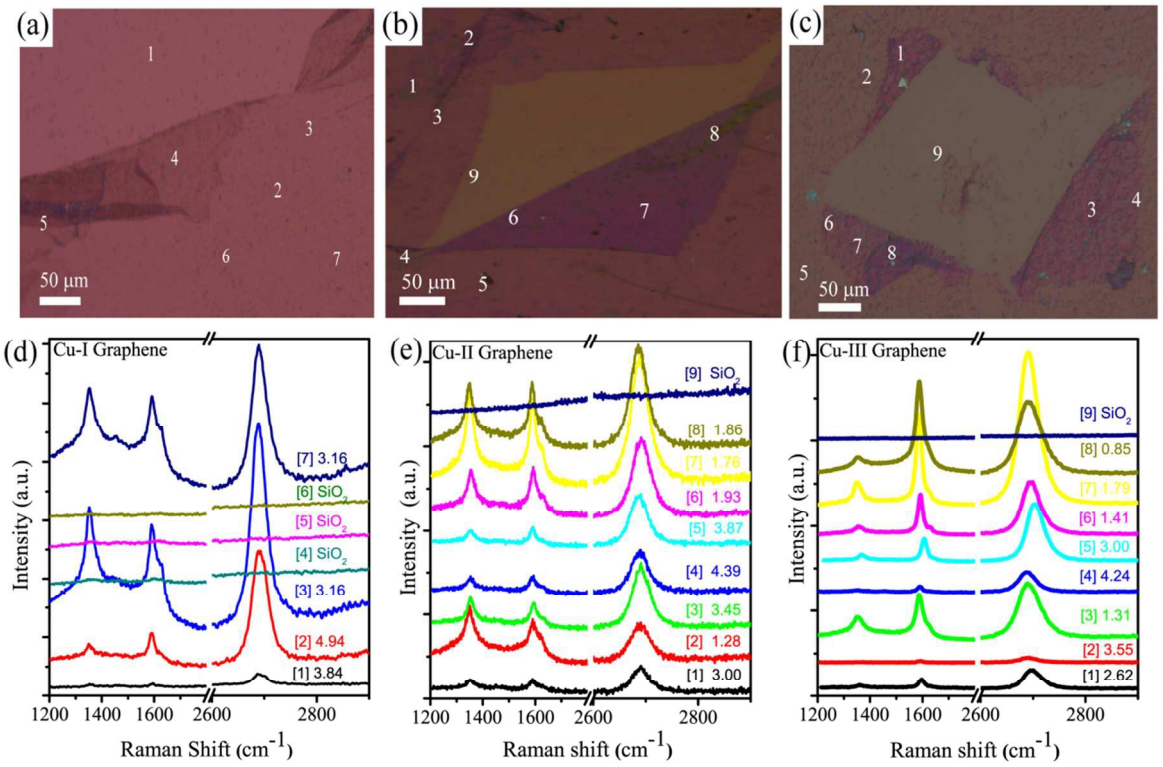

Fig 4: Optical micrographs of transferred graphene with different marked positions (a) Cu-I graphene, (b) Cu-II graphene and (c) Cu-III graphene. (d)- (f) Corresponding Raman Spectra as marked in (a), (b) and (c) respectively.

To understand the difference in the crystallinity and defect density of the graphene grown over three substrates with varying purity, we probed the role of substrates crystallinity, its surface planes and its evolution during annealing and growth using XRD. Fig. 5(a) shows the XRD pattern of cleaned substrates Cu-I, Cu-II and Cu-III recorded using Bragg-Bento geometry and Cu $K\alpha_1$ line. Cleaned Cu-I and Cu-II substrate shows peaks corresponding to (111), (100), (110),

(311) and (400), While Cu-III shows peaks corresponding to (111), (100) and (311). Peaks corresponding to (110) and (400) were not observed in case of Cu-III substrate. In case of Cu-I and Cu-II peak corresponding to (100) lattice plane shows highest intensity while in case of Cu-III, peak corresponding to (111) lattice facet shows highest intensity. Fig. 5 (b) shows XRD pattern of Cu-I substrate after cleaning (black curve), after annealing at 1000°C for 30 mins (red curve) and after growth for 10 mins (blue curve). The relative peak intensity of (111) and (100) peaks changes significantly upon annealing for 30 minutes before growth. In case of cleaned Cu-I substrate the (100) peak has highest peak intensity while upon annealing (111) peak becomes more intense than (100) peak.

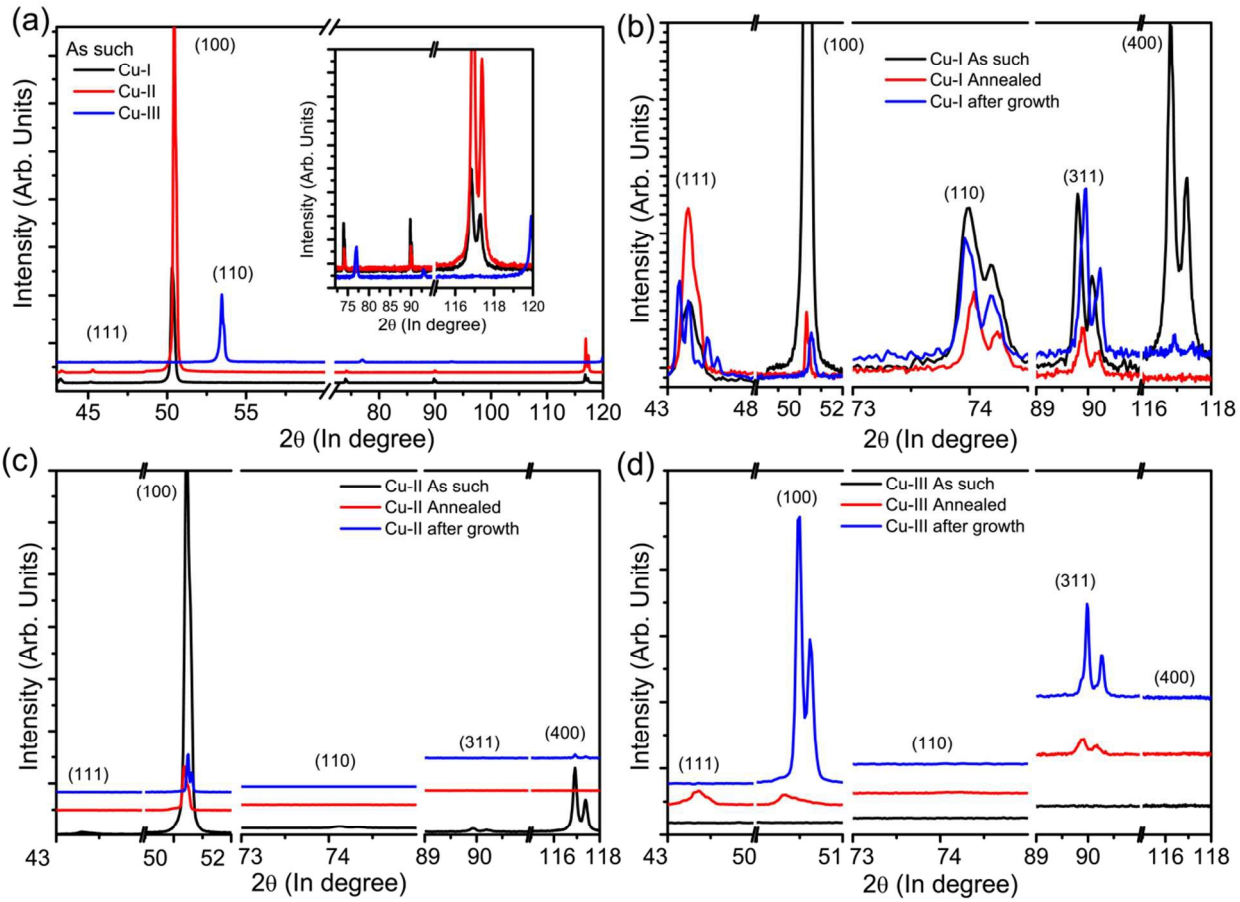

Fig 5: X-ray diffraction pattern of copper substrates as such, annealed and after growth. (a) Cleaned copper substrate of the three copper foil, (b) Cu-I, (c) Cu-II and (d) Cu-III.

This shows that in Cu-I after annealing at 1000°C for 30 minute (at low pressure < 100 mtorr), the preferred crystal plane of for growth is (111). The peak intensity of (100), (110), (311) and

(400) planes are suppressed upon annealing. The relative change in the peak intensity of various planes occurs due to the high degree of mobility of copper atoms at elevated temperature of 1000 º C (i.e. only 83 ºC less than the Cu melting point) leading to merging of facets. The XRD spectra of Cu-I graphene sample (i.e., after 10 mins growth on annealed substrate at pressure 0.29 torr) shows splitting of (111) peak into multiple components. This represents varying percentage of compressive strain along the (111) plane and is the most favored plane for growth among all other [26]. Reflection from the lattice planes (100) and (311) also shows shift to higher Bragg angles upon growth, representing compressive strain along these planes as well.

Fig. 5(c) shows XRD pattern of Cu-II after cleaning (black curve), after annealing (red curve) and after graphene growth (blue curve). In case of Cu-II (100) facet is most prominent before annealing analogous to the Cu-I. In addition to it, cleaned Cu-II substrate consists of (111), (110), (311) and (400) planes. After annealing Cu-II, only (100) plane is observed and reflections from (111), (110) and (400) is of negligible intensity. The (100) peak shifted to lower Bragg angle upon annealing and it shows multiple splitting after growth and shifts to higher Bragg angle. In addition to (100) peak, (400) appears with weak intensity after growth. Although the cleaned Cu-I and Cu-II substrates initially showed similar diffraction pattern initially i.e (111), (100) (110), (311) and (400) but after annealing, depending upon substrates purity level they behave differently.

Fig. 5(d) shows XRD pattern of Cu-III after cleaning, after annealing and after graphene growth. The cleaned Cu-III substrate consists of peak at 2θ value 53.45, 77.00 and at 92.90° which are located at different position than the peaks observed in case of Cu-I and Cu-II. These peaks are close to the assigned planes (100), (110) and (311) peak observed in case of Cu-I and Cu-II. Peaks at 2θ value 53.45, 77.00 and 92.90° are located at higher Bragg angles than expected peaks at 2θ= 50.33, 74.20 and 89.90° corresponding to (100), (110) and (311) planes indicating presence of compressive strain along with these planes. After annealing peak corresponding to (111) plane shows maximum intensity while (100) and (311) plane shifts towards lower Bragg angles at the expected peak values similar to Cu-I and Cu-II. After growth, the XRD pattern of Cu-III shows reflections of (100) and (311) planes. The (111) plane shows negligibly small intensity after growth, although it had been prominent after annealing. This make it difficult to

comment whether (111) plane participates during growth or not. After growth, (100) plane shows splitting of peak indicating its larger participation in graphene growth. The behavior of the Cu-III is analogous to the Cu-II where growth is from (100) lattice plane, while it differs from Cu-I where it occurs from (111) plane. This indicates that as the purity of the substrate used increases the growth begins to favors (100) lattice plane relative to the (111) plane.

XRD line profile of Cu-I shows that it contains large number of different facet steps and grain boundaries having high activation energy for hydrocarbon decomposition that acts as graphene nucleation site[35]. Due to these characteristics in case of Cu-I, annealing and growth restricted the mobility of Cu atom at low pressure condition and resulted into growth of graphene in particular crystallographic plane Cu (111) as evidenced by XRD Fig 5(b). It has been suggested that symmetry of (111) surface of FCC crystal is of flat hexagonal atomic arrangement similar to graphene and have low surface energy with high diffusion rate that promote hexagonal superstructure of graphene with good uniformity. It is observed that although optical image shows continuous graphene sheet but Raman spectra demonstrate that in all the marked location the peaks of graphene does not appear (marked by number 1, 2 and 3 Figure 4(d)). This confirms that the graphene sheet is of discontinuous in nature due to the nucleation of graphene at various sites and it is consequence of low purity. In all the location the $I_{G'}/I_G \approx 3$(between 2.5 to 5.0) corresponding to the single layer graphene. Discontinuity in graphene sheet primarily comes from the polycrystalline nature of substrate and dissimilarity of crystal structure of graphene with underlying copper crystal. Terminated grain boundaries in polycrystalline substrate lead to the formation of high density graphene seed in various nucleation sites that finally result in the formation of graphene grain boundary. Since graphene grain boundaries are prone to manifestation of damage in individual sheet resulting into the irregular graphene sheet from Cu-I.

Graphene produced using Cu-II is monolayer in nature as indicated by $I_{G'}/I_D$ ratio of 3.9. In addition to it, high value of I_D/I_G ratio for Cu-II graphene signifies that graphene grains are divergence with the square surface symmetry of Cu (100) facet. Hence the quality of graphene grown on Cu-II substrate is comparatively more imperfect in reference to (I_D/I_G) ratio as well as the D peak intensity is significantly high as compared to graphene sheet grown on Cu-I and Cu-

III. The high defect density ~ 2320 μm^{-2} may be due to the mismatch in the crystallographic plane of square Cu(100) plane and hexagonal structure of graphene over the Cu substrate. Also the presence of different graphene orientations on Cu (100) would cause defects at the graphene grain boundaries when graphene islands meet and grow[46]. The Raman spectroscopic data at different location with corresponding optical image in Fig 4(b) confirms that the graphene sheet grown on Cu-II is dominantly monolayer in nature in which the $I_{G'}/I_G$ ratio in more than 3 and FWHM is in between 20-30 cm^{-1}. While the Raman spectra in the folded region shows increase in the intensity of the D peak due to increased number of intra valley electrons scattering through K-point. This results into decreases of $I_{G'}/I_G$ intensity ratio since the folded graphene layer behaves like double layer graphene ($I_{G'}/I_G < 2$). In case of medium (Cu-II) and high purity (Cu-III) high defect intensity arises from lattice mismatch originated due to graphene and participative Cu plane (100).

Conclusions

The present study demonstrated that irrespective of the purity of the copper substrate, monolayer graphene can be grown as indicated by $I_{G'}/I_G$ ratio which is ~ 4. However, purity of the substrate plays a noteworthy role towards the quality of the graphene. The Cu substrate with higher purity (Cu-III) shows larger grain size under similar annealing and growth conditions. The Raman spectra of graphene confirm that Cu-II substrate with intermediate purity (99.8 %) shows high defect density (≈ 2320 μm^{-2}) along with highest crystallinity ($I_{G'}/I_G$). Also Raman spectra reveal that with increasing substrate purity the peak position G and G´-band monotonically blue-shifted indicating higher tensile strain. The single layer growth on lowest purity Cu substrate but continuous sheet formation is missing in contrast to high purity copper substrates used (Cu-II and Cu-III). With increasing purity of Cu substrate used, the formation of continuous monolayer graphene sheet increases. XRD studies attributes that growth occurs in Cu-I preferably from (111) plane, while in case of intermediate purity Cu-II the favored plane for growth is (100). In case of substrate/ highest purity Cu-III, the preferred plane for growth is indecisive to decide as the (111) plane peak shows highest intensity but after growth (100) plane becomes most intense. We expect that in highest purity substrate growth begins with (111) plane but mobility of Cu-atoms during growth process favors evolution of (100) plane on the top surface. With increasing the purity of the substrate the growth favors (100) plane and (100) plane assisted growth results

into larger size crystallites of grown graphene. The cubic surface crystallographic of (100) facet in Cu-II results into more defect density in the grown graphene due to the mismatch in crystallographic plane of substrate and graphene. This kind of study unveils the recipe to grow graphene sheet with larger crystallize size for device applications. The investigation gives us detailed insight information of how Cu-crystal plane and its purity help in determination of the graphene quality on the basis of XRD-pattern and Raman spectroscopic analysis.

Acknowledgment

The authors are grateful to Director, CSIR-National Physical Laboratory, and New Delhi for encouragement and permission to publish this work. The authors are also grateful to Mrs. S. Sharma for doing Raman Spectroscopy of the graphene sample, Mr. Jai Tawale for providing SEM analysis and Dr. V.P.S. Awana for X-ray characterization. Author Munu Borah would like to thanks Department of Science and Technology for financial assistant under Women Scientist (WOS-A/CS-90/2011) scheme.

Supporting Information Available:

References:

1. S. P. Koenig, L. Wang, J. Pellegrino and J. S. Bunch, *Nature nanotechnology*, 2012, **7**, 728-732.
2. S. Garaj, W. Hubbard, A. Reina, J. Kong, D. Branton and J. Golovchenko, *Nature*, 2010, **467**, 190-193.
3. S. Garaj, S. Liu, J. A. Golovchenko and D. Branton, *Proceedings of the National Academy of Sciences*, 2013, **110**, 12192-12196.
4. C. A. Merchant, K. Healy, M. Wanunu, V. Ray, N. Peterman, J. Bartel, M. D. Fischbein, K. Venta, Z. Luo and A. C. Johnson, *Nano letters*, 2010, **10**, 2915-2921.
5. K. I. Bolotin, K. Sikes, Z. Jiang, M. Klima, G. Fudenberg, J. Hone, P. Kim and H. Stormer, *Solid State Communications*, 2008, **146**, 351-355.
6. J. Moser, A. Barreiro and A. Bachtold, *Applied Physics Letters*, 2007, **91**, 163513.
7. Z.-S. Wu, W. Ren, L. Gao, J. Zhao, Z. Chen, B. Liu, D. Tang, B. Yu, C. Jiang and H.-M. Cheng, *Acs Nano*, 2009, **3**, 411-417.
8. A. C. Neto, F. Guinea, N. Peres, K. S. Novoselov and A. K. Geim, *Reviews of modern physics*, 2009, **81**, 109.
9. K. Novoselov, D. Jiang, F. Schedin, T. Booth, V. Khotkevich, S. Morozov and A. Geim, *Proceedings of the National Academy of Sciences of the United States of America*, 2005, **102**, 10451-10453.
10. Y.-M. Lin, C. Dimitrakopoulos, K. A. Jenkins, D. B. Farmer, H.-Y. Chiu, A. Grill and P. Avouris, *Science*, 2010, **327**, 662-662.
11. S. Dhakate, N. Chauhan, S. Sharma, J. Tawale, S. Singh, P. Sahare and R. Mathur, *Carbon*, 2011, **49**, 1946-1954.

12. S. Bae, H. Kim, Y. Lee, X. Xu, J.-S. Park, Y. Zheng, J. Balakrishnan, T. Lei, H. R. Kim and Y. I. Song, *Nature nanotechnology*, 2010, **5**, 574-578.
13. X. Li, W. Cai, J. An, S. Kim, J. Nah, D. Yang, R. Piner, A. Velamakanni, I. Jung and E. Tutuc, *Science*, 2009, **324**, 1312-1314.
14. H. Song, S. Li, H. Miyazaki, S. Sato, K. Hayashi, A. Yamada, N. Yokoyama and K. Tsukagoshi, *Scientific reports*, 2012, **2**.
15. A. K. Geim and K. S. Novoselov, *Nature materials*, 2007, **6**, 183-191.
16. P. Dharmaraj, K. Jeganathan, V. Gokulakrishnan, P. Sundara Venkatesh, R. Parameshwari, V. Ramakrishnan, S. Balakumar, K. Asokan and K. Ramamurthi, *The Journal of Physical Chemistry C*, 2013, **117**, 19195-19202.
17. X. Li, C. W. Magnuson, A. Venugopal, R. M. Tromp, J. B. Hannon, E. M. Vogel, L. Colombo and R. S. Ruoff, *Journal of the American Chemical Society*, 2011, **133**, 2816-2819.
18. C. Mattevi, H. Kim and M. Chhowalla, *Journal of Materials Chemistry*, 2011, **21**, 3324-3334.
19. C.-M. Seah, S.-P. Chai and A. R. Mohamed, *Carbon*, 2014, **70**, 1-21.
20. W.-G. Lee, E. Kim and J. Jung, *Materials chemistry and physics*, 2014, **147**, 452-460.
21. J. Wang, M. Zeng, L. Tan, B. Dai, Y. Deng, M. Rümmeli, H. Xu, Z. Li, S. Wang and L. Peng, *Scientific reports*, 2013, **3**.
22. D. Geng, L. Meng, B. Chen, E. Gao, W. Yan, H. Yan, B. Luo, J. Xu, H. Wang and Z. Mao, *Advanced Materials*, 2014, **26**, 6423-6429.
23. Y. Liang, L. Yu, Z. Cui, S. Zhu, Z. Li and X. Yang, *Science of Advanced Materials*, 2014, **6**, 545-549.
24. P. R. Kidambi, C. Ducati, B. Dlubak, D. Gardiner, R. S. Weatherup, M.-B. Martin, P. Seneor, H. Coles and S. Hofmann, *The Journal of Physical Chemistry C*, 2012, **116**, 22492-22501.
25. Y. Ogawa, B. Hu, C. M. Orofeo, M. Tsuji, K.-i. Ikeda, S. Mizuno, H. Hibino and H. Ago, *The Journal of Physical Chemistry Letters*, 2012, **3**, 219-226.
26. H. I. Rasool, E. B. Song, M. J. Allen, J. K. Wassei, R. B. Kaner, K. L. Wang, B. H. Weiller and J. K. Gimzewski, *Nano letters*, 2010, **11**, 251-256.
27. J. D. Wood, S. W. Schmucker, A. S. Lyons, E. Pop and J. W. Lyding, *Nano letters*, 2011, **11**, 4547-4554.
28. I. Vlassiouk, M. Regmi, P. Fulvio, S. Dai, P. Datskos, G. Eres and S. Smirnov, *Acs Nano*, 2011, **5**, 6069-6076.
29. W. Liu, H. Li, C. Xu, Y. Khatami and K. Banerjee, *Carbon*, 2011, **49**, 4122-4130.
30. X. Li, C. W. Magnuson, A. Venugopal, J. An, J. W. Suk, B. Han, M. Borysiak, W. Cai, A. Velamakanni and Y. Zhu, *Nano letters*, 2010, **10**, 4328-4334.
31. Q. Yu, L. A. Jauregui, W. Wu, R. Colby, J. Tian, Z. Su, H. Cao, Z. Liu, D. Pandey and D. Wei, *Nature materials*, 2011, **10**, 443-449.
32. R. Viswanathan and C. Bauer, *Metallurgical Transactions*, 1973, **4**, 2645-2650.
33. S. Najmaei, Z. Liu, W. Zhou, X. Zou, G. Shi, S. Lei, B. I. Yakobson, J.-C. Idrobo, P. M. Ajayan and J. Lou, *Nature materials*, 2013, **12**, 754-759.
34. A. C. Ferrari and D. M. Basko, *Nature nanotechnology*, 2013, **8**, 235-246.
35. R. Saito, A. Grüneis, G. G. Samsonidze, V. Brar, G. Dresselhaus, M. Dresselhaus, A. Jorio, L. Cançado, C. Fantini and M. Pimenta, *New Journal of Physics*, 2003, **5**, 157.
36. M. S. Dresselhaus, G. Dresselhaus, R. Saito and A. Jorio, *Physics reports*, 2005, **409**, 47-99.
37. K. K. Kim, J. S. Park, S. J. Kim, H. Z. Geng, K. H. An, C.-M. Yang, K. Sato, R. Saito and Y. H. Lee, *Physical Review B*, 2007, **76**, 205426.
38. J. Park, A. Reina, R. Saito, J. Kong, G. Dresselhaus and M. Dresselhaus, *Carbon*, 2009, **47**, 1303-1310.
39. S. Bhaviripudi, X. Jia, M. S. Dresselhaus and J. Kong, *Nano letters*, 2010, **10**, 4128-4133.

40. L. G. Cançado, A. Jorio, E. M. Ferreira, F. Stavale, C. Achete, R. Capaz, M. Moutinho, A. Lombardo, T. Kulmala and A. Ferrari, *Nano letters*, 2011, **11**, 3190-3196.
41. C. Hu, S. Sedghi, A. Silvestre-Albero, G. G. Andersson, A. Sharma, P. Pendleton, F. Rodríguez-Reinoso, K. Kaneko and M. J. Biggs, *Carbon*, 2015, **85**, 147-158.
42. R. K. Biroju and P. Giri, *The Journal of Physical Chemistry C*, 2014, **118**, 13833-13843.
43. A. C. Ferrari, *Solid State Communications*, 2007, **143**, 47-57.
44. L. Tao, J. Lee, M. Holt, H. Chou, S. J. McDonnell, D. A. Ferrer, M. G. Babenco, R. M. Wallace, S. K. Banerjee and R. S. Ruoff, *The Journal of Physical Chemistry C*, 2012, **116**, 24068-24074.
45. Z. Ni, Y. Wang, T. Yu, Y. You and Z. Shen, *Physical Review B*, 2008, **77**, 235403.
46. L. Zhao, K. Rim, H. Zhou, R. He, T. Heinz, A. Pinczuk, G. Flynn and A. Pasupathy, *Solid State Communications*, 2011, **151**, 509-513.